This is an open access article published under a Creative Commons Attribution (CC-BY) License, which permits unrestricted use, distribution and reproduction in any medium, provided the author and source are cited.

ACS Catalysis

Perspective

pubs.acs.org/acscatalysis

Understanding Immobilized Molecular Catalysts for Fuel-Forming Reactions through UV/Vis Spectroelectrochemistry

Timothy E. Rosser and Erwin Reisner*

Christian Doppler Laboratory for Sustainable SynGas Chemistry, Department of Chemistry, University of Cambridge, Lensfield Road, Cambridge CB2 1EW, U.K.

ABSTRACT: Molecular catalysis of fuel-forming half reactions such as proton and CO_2 reduction is a key area of study for achieving electrical-to-chemical energy storage and solar fuel synthesis. Immobilization of these molecular catalysts on electrode surfaces often results in high turnover numbers and selectivities, even under the challenging conditions of an aqueous environment. This Perspective considers how the combination of electrochemistry and electronic spectroscopy can be used to characterize catalytic processes *in operando*, explaining the observed performance and therefore guiding the design principles for the next generation of material/molecule hybrid electrodes and devices. Numerous immobilization strategies and electrode materials are already available, of which wide band gap metal oxides offer transparency to visible light and are therefore ideal for spectroelectrochemical characterization. Spectroscopic analysis of emerging catalytic metal−organic framework and polymer films is also discussed.

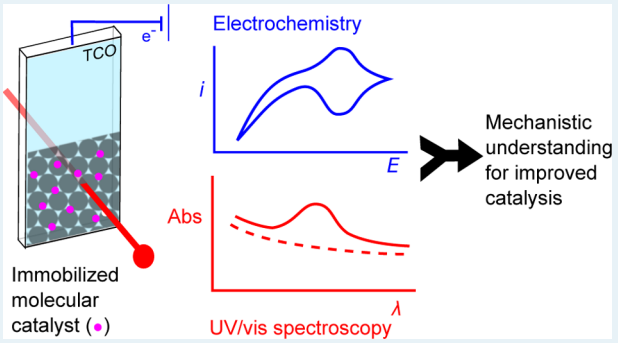

KEYWORDS: *spectroelectrochemistry, proton reduction, CO_2 reduction, electrocatalysis, molecular catalysis*

1. INTRODUCTION

The conversion of abundant resources of water, CO_2, and solar light into fuel and feedstock chemicals, as achieved in natural photosynthesis, is attractive for sustainable economic development. Research on artificial photosynthesis focuses typically on solar light harvesting combined with catalysis of the proton/CO_2 reduction and H_2O oxidation reactions and results in systems with ever increasing solar-to-fuel conversion efficiencies.[1−3] The optimal coupling of light harvesting[4] with catalytically active materials requires minimized charge recombination and therefore maximized energy storage efficiency. This Perspective focuses on the mechanistic understanding of molecular electrocatalysts interfaced with electrodes, which is essential for applications of artificial photosynthesis. In particular, we will consider how electrochemical techniques can be combined with spectroscopy to improve our understanding of hybrid molecular catalysts/solid state materials and advance the development of solar fuels devices.

Electrocatalysis of fuel-forming reactions (proton and CO_2 reduction) sources electrons from an electrochemical circuit, offering the opportunity to avoid potentially complicating chemical reducing reagents. Performing these reactions using molecularly defined transition metal coordination compounds is an attractive area of study with several advantages compared to classical solid-state counterparts. First, molecular metal complexes offer distinct spectroscopic handles for a well-defined catalytic site, which can be used to infer mechanistic insights about the catalytic cycle and the overall fuel-forming system. Moreover, the exquisite control offered by modern synthetic chemistry on molecular structure allows any bottlenecks identified by such spectroscopic studies to be overcome by catalyst modification.[5,6] Molecular catalysis is vital in performing selective reactions for chemically complex transformations such as CO_2 and N_2 reduction, where a variety of products are possible without rigorous catalytic control.[7−9] The principles developed by studying artificial photosynthetic systems can also be applied to more specificity-demanding reactions in organic photocatalysis that require molecular catalysts.[10]

Finally, the study of molecular electrocatalysis has a synergistic relationship with enzyme redox catalysis, with H_2-producing hydrogenase enzymes also being deployed in solar fuels devices such as those shown in Figure 1.[11,12] The structures of enzyme active sites provide inspiration for the synthesis of efficient synthetic catalysts,[13,14] and spectroscopic investigations of small molecule enzyme mimics are used to learn about the structure and activity[15,16] of the enzymes themselves. Currently, immobilized molecular electrocatalysts for fuel-forming reactions are typically studied *in operando* by UV/vis spectroelectrochemistry, whereas related enzymes such as hydrogenases[17,18] and nitrogenases[19] are studied using vibrational spectroscopic and electron paramagnetic resonance techniques,[20,21] with an exception being the study of electron

Received: January 31, 2017
Revised: March 17, 2017
Published: March 21, 2017

 © 2017 American Chemical Society

DOI: 10.1021/acscatal.7b00326
ACS Catal. 2017, 7, 3131−3141

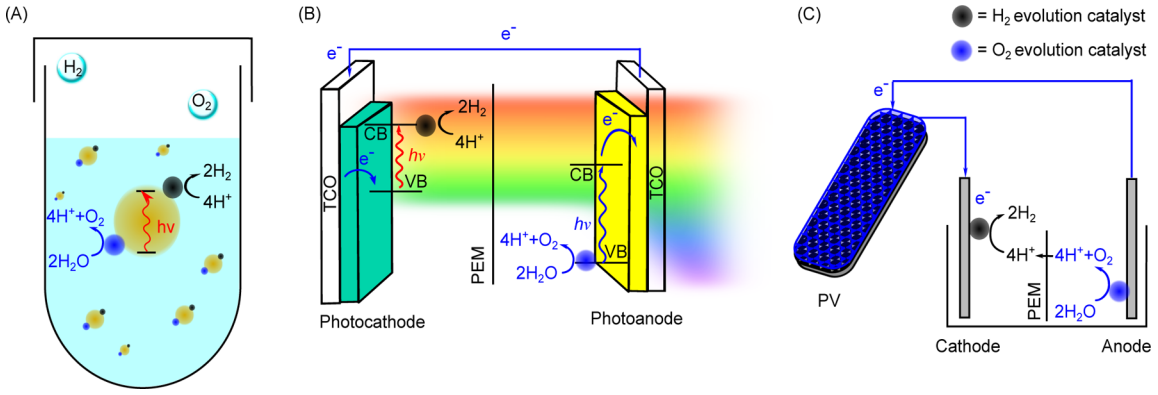

Figure 1. Schematic representation of (A) suspension, (B) PEC, and (C) PV/electrolysis architectures for solar fuel synthesis.

transport through an $[Fe_4S_4]$ cluster in CO dehydrogenase by UV/vis spectroelectrochemistry.[22] The examples highlighted herein for the study of immobilized synthetic catalysts by UV/vis spectroelectrochemistry may also provide inspiration for the study of enzyme electrocatalysis in the future.

Achieving artificial photosynthesis requires consideration on a micro- and macroscopic scale. Three classes of device have been proposed for full water splitting,[23,24] although the proton reduction half reaction could be replaced with CO_2 reduction without significant alteration to the overall device configuration (Figure 1):

A. One-pot systems comprising a light absorber in solution or suspension, with oxidation and reduction reactions performed by two molecular catalysts in the same vessel ("particle-based system").[3] These systems are potentially the simplest to implement but suffer from the limitation of production of oxidized and reduced products in the same compartment. This can lower efficiency by leading to deleterious short-circuit reactions, as well as creating potentially explosive gas mixtures. Closed redox reactions with molecular catalysts in semihomogeneous suspension have been achieved thus far for alcohol and phosphine oxidation in combination with H_2 production with a molecular catalyst.[25,26]

B. Photoelectrochemical (PEC) cells comprising two semiconductor photoelectrodes absorbing complementary portions of the solar spectrum combined with immobilized catalysts performing oxidative and reductive half reactions in separate compartments, leading to straightforward product separation.[27] Full PEC water splitting has recently been achieved by molecular catalysts immobilized on metal oxide electrodes,[28−30] but this approach requires the components to be operable under the same benign conditions, limiting the possible light harvester and catalyst combinations.

C. Photovoltaic devices coupled with electrolysis cells with oxidation and reduction reactions operating independently of light ("PV/electrolysis").[31] This offers the advantage of independent optimization of light harvesting and catalysis, allowing systems where these components have orthogonal stabilities. Moreover, electrolysis cells can be combined with alternative renewable electricity sources to PV where this is more practical. Electrolysis cells for CO_2 splitting (CO_2 reduction combined with H_2O oxidation) with molecular oxidation and reduction catalysts are already achieving overall energy efficiencies approaching 50%,[5,32] and molecular H_2 production cathodes have also displayed high activity under conditions relevant to electrolysis cells.[33]

In all of these cases, the direct attachment of the catalysts to either light-harvesting or electrode materials is important for making the most efficient use of the catalytic centers, by avoiding inactive catalysts in the bulk solution and kinetic limitations of diffusion. This is particularly important for designs B and C, where the overall reaction is split into two half reactions on electrodes. Attachment of the catalyst to the electrode, referred to herein as 'immobilization,' prevents diffusion of oxidized or reduced compounds into the bulk solution and to the counter electrode, thus avoiding short circuit reactions and maximizing efficiency. This Perspective focuses on the study of molecular catalysts immobilized on surfaces without freely diffusing catalyst in the electrolyte solution, progress from which will help improving the efficiencies of all the above architectures.

A particular advantage of attaching molecular catalysts to electrode surfaces is that it provides a platform to study the catalyst itself under conditions in which they are most effective. The absence of catalyst diffusion means catalytic centers are constantly turning over under the application of a suitable electrochemical potential. Therefore, *in operando* characterization is performed only on material undergoing catalysis.[30] Since immobilization positions the catalysts at the electrode surface, electrochemically induced changes affect the whole sample instantaneously, so these systems are ideal for simultaneous spectroscopic characterization since the signal is not masked by unreacted catalyst in the bulk solution.

A potential disadvantage of this approach is that a monolayer of molecular catalyst, which is desirable for nondiffusional electronic communication and efficiently employing the available metal centers, results in the use of tiny amounts of catalyst on the accessible (effective) surface area for spectroscopic measurements. Consequently, such measurements are often close to the sensitivity limit, and species formed in low concentrations may not be detectable. A possible solution is to develop nanostructured, high surface area electrode materials, a monolayer on which will position more molecules within the two-dimensional (geometric) sample area. Nanostructuring offers the dual advantage of higher current densities and therefore product formation per geometric area, and many examples have made use of this strategy.[5,30,34−36] An alternative approach would be to use a surface-sensitive spectroscopic technique such as surface-enhanced resonance Raman spectroelectrochemistry for *in situ* characterization,[37,38] although this approach shall not be considered in this Perspective as it has yet to be applied to immobilized molecular electrocatalysis of proton or CO_2 reduction.

DOI: 10.1021/acscatal.7b00326
ACS Catal. 2017, 7, 3131−3141

With the above considerations, this Perspective will discuss the application of UV/vis spectroelectrochemistry to immobilized molecular fuel forming electrocatalysis to aid understanding of the catalytic mechanism and therefore improve activity. The discussion will be limited to the UV/vis region because this allows characterization of electronic transitions in near-ubiquitous transition metal centers, and this technique is sensitive to changes in the oxidation state, which is particularly important in redox catalysis. Water oxidation electrocatalysis will not be included in detail, because the metal-oxo multiple bonds formed during the catalytic mechanism are better suited to study by resonance Raman techniques, and this topic has already been reviewed elsewhere.[39]

2. IMMOBILIZED MOLECULAR CATALYSTS IN ELECTROCATALYTIC FUEL PRODUCTION

Immobilized molecular electrocatalysis necessitates a durable chemical attachment strategy for the chosen catalyst to the electrode material. Strategies used to attach molecular proton and CO_2 reduction catalysts to surfaces include using the unfunctionalized molecule directly immobilized through hydrophobicity[5] or a polymer matrix,[40−42] growth of molecular framework materials,[14] direct covalent bonding,[43,44] $\pi-\pi$ interactions,[45,46] and the interaction between phosphonic acids, carboxylic acids, and other anchoring groups with metal oxides.[47−49] These approaches have been recently reviewed for proton[50] and CO_2[51] reduction, and this Perspective will consider cases where complementary *in operando* spectroscopic and electrochemical data have been used to draw conclusions and mechanistic insights regarding the activity of molecule/electrode hybrid systems.

An inert, stable, and conducting electrode material with potential for chemical functionalization and a high effective surface area facilitates immobilized molecular catalysis. To this end, carbon based materials have been extensively explored for the immobilization of modified molecular catalysts for proton and CO_2 reduction, particularly due to the high surface areas offered by arrays of carbon nanotubes.[50] This has included direct grafting and supramolecular modification of carbon surfaces and is associated with high electrocatalytic turnover numbers compared to the catalysts operating in homogeneous solution.[45,52] However, the carbon nanotubes have typically been deposited on glassy carbon or gas diffusion layers, which precluded transmission spectroscopic studies of the reactive intermediates due to lack of optical transparency of the electrodes. In addition, even on support-free buckypaper electrodes, a dense forest of carbon nanotubes blocks light and makes spectroscopic studies challenging.[42] Nevertheless, purely electrochemical techniques have enabled some mechanistic deductions.[41,46]

2.1. Immobilization on Metal Oxide Electrodes.

Transparent conducting oxide (TCO) materials such as indium tin oxide (ITO) offer the conductivity necessary to perform electrochemical investigations, alongside transparency to visible light to perform transmission electronic absorption spectroscopy. Moreover, mesoporous and macroporous inverse-opal ITO electrodes can be readily prepared,[12,53] achieving high surface areas and thereby current densities with immobilized catalysts (Figure 2). Immobilization of the appropriately modified molecular catalyst can then be achieved by simple drop-casting or submersion for a number of hours followed by rinsing of excess catalyst. This strategy tends to rely on the interaction between molecules modified with carboxylic and

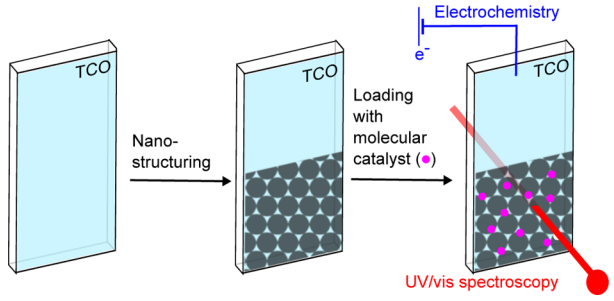

Figure 2. Schematic representation for preparation of a porous metal oxide scaffold (such as ITO or TiO_2) on TCO-coated glass, followed by modification with a molecular catalyst for *in situ* spectroelectrochemical studies.

phosphonic acid linkers and metal oxide surfaces,[48] leading to the subsequent construction of TCO-dye-catalyst assemblies through the use of supramolecular linkers such as Zr^{4+} and host−guest interactions.[54−56] This level of control is not always offered by other approaches such as covalent immobilization, where submonolayer coverages may limit the overall current density,[52] and polymerization, where multilayer films with limited conductivity can hinder electrochemical characterization.[57,58]

Cobalt compounds bearing multidentate oxime and related ligands are well studied for H_2 production in homogeneous solution,[59−61] in particle suspensions,[49,62] and more recently covalently attached to electrode surfaces.[6,34,63] However, the mechanism for the catalytic reaction has been controversal,[64] including whether the molecular mechanism is mono- or bimolecular or if the molecular structure of the catalyst is even retained during prolonged electrocatalysis.[65−67] Immobilization has resulted in the highest turnover numbers from these highly active catalytic cores,[63] but since immobilization results in drastic changes to the chemical environment, it is essential to complement these investigations with *in operando* mechanistic studies.

Phosphonic acid groups are well known to attach to metal oxide surfaces under acidic and pH neutral conditions,[68] and the series of Co-based catalysts **CoP^1**, **CoP^2**, and **CoP^3** (Figure 3) incorporates phosphonic acid anchoring groups for immobilization.[6,34,69] The first-generation cobaloxime compound **CoP^1** produced H_2 photocatalytically from aqueous protons on dye-sensitized TiO_2 particles[70] and electrocatalytically in homogeneous solution[71] (even in the presence of O_2)[70,72] and was therefore immobilized on mesoporous ITO (mesoITO) electrodes for more detailed investigations into the behavior of the immobilized catalysts. Cyclic voltammetry (CV) of these hybrid electrodes in aqueous solution revealed an initial reduction wave assigned to $Co^{III/II}$ followed by an electrocatalytic wave at more reducing potentials representing H_2 production.[6] However, these CV features diminished within a few scans, and discoloration of the mesoITO electrode indicated loss of the catalytic centers from the electrode surfaces due to the lability of the Co-pyridine bond during the catalytic cycle,[67] although some equatorial ligand degradation may also occur, as suggested by the restoration of activity upon readdition of excess dimethylglyoxime equatorial ligand to **CoP^1** in a dye-sensitized photocatalytic suspension.[71]

The diimine-dioxime compound **CoP^2** instead incorporated the phosphonic acid anchoring group into the pseudomacrocyclic equatorial ligand backbone for more robust immobiliza-

DOI: 10.1021/acscatal.7b00326
ACS Catal. 2017, 7, 3131−3141

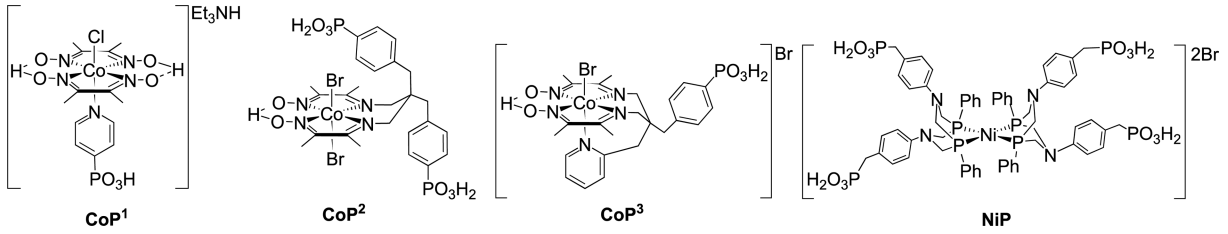

Figure 3. Phosphonic acid-modified cobalt tetra-imine[6,34,69] and nickel bis(diphosphine)[30] H_2 evolution catalysts.

tion and was studied for electrocatalytic H_2 production on mesoITO electrodes with a high surface coverage of 150 nmol cm^{-2} (geometric surface area).[34] Upon scanning to cathodic potentials in DMF electrolyte solution, CV revealed two reduction events assigned to the reduction of the parent Co^{III} compound to Co^{II} and Co^{I} by UV/vis spectroelectrochemistry (Figure 4A and Figure 4B).[73] The spectral features showed no signs of desorption over 2 h, demonstrating good electronic communication and stability offered between the phosphonic acid linkers and the ITO surface under these conditions. When these spectroelectrochemical experiments were performed in aqueous solution, the same species were identified when the electrodes were negatively polarized (Figure 4C). The electronic transition at λ_{abs} = 655 nm, corresponding to Co^{I}, disappeared within a few seconds of applying the potential under catalytically relevant conditions, although a redox wave corresponding to $Co^{III/II}$ was still observed in subsequent CV scans. The identification of waves in the return scan indicated that the attachment between **CoP²** and the surface was also stable under aqueous catalytic conditions and that the reason for the depletion Co^{I} under an applied catalytically relevant potential was proton reduction with concomitant oxidation of the cobalt center. Therefore, the combination of UV/vis spectroscopy with electrochemistry enabled the study of the durability of the catalyst immobilization on an electrode surface, as well as the identification of the active species for proton reduction. The same Co oxidation states have been spectroelectrochemically identified for a cobaloxime compound immobilized on mesoITO electrodes by coordination to a poly(vinylpyridine) polymer in both aqueous and nonaqueous conditions.[74]

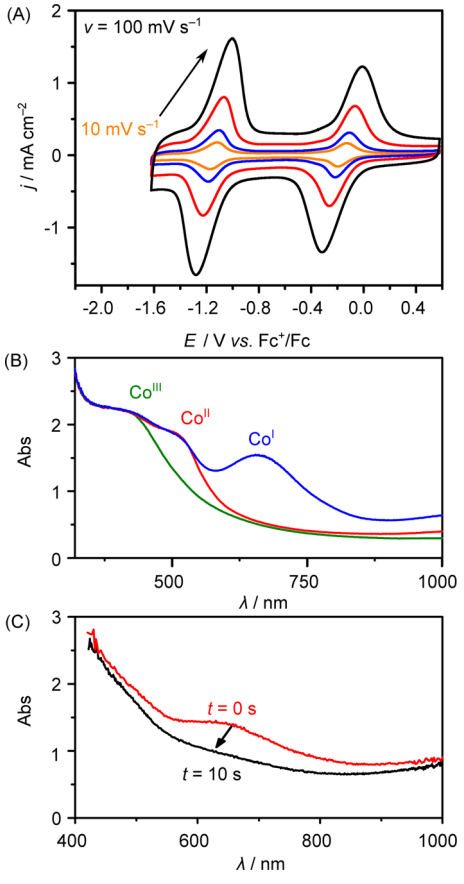

Figure 4. (A) CV scans of **CoP²** immobilized on mesoITO in DMF electrolyte solution at different scan rates. Adapted from ref 6. (B) UV/vis spectra of electrochemically generated oxidation states of cobalt for mesoITO|**CoP²** in DMF electrolyte solution. (C) Spectroelectrochemistry of mesoITO|**CoP²** in aqueous electrolyte solution (pH 7) immediately upon application of E = −0.6 V vs NHE and after 10 s at this potential. Arrow indicates the sequence of measurements. Adapted with permission from ref 34. Copyright 2012 Wiley-VCH Verlag GmbH & Co. KGaA.

The next-generation catalyst, **CoP³** (Figure 3), was synthesized with one of the phosphonic acid linkers of **CoP²** being replaced with a pyridine moiety that can coordinate axially to the Co center.[6] This modification led to substantially improved photocatalytic H_2 production when **CoP³** was immobilized on Ru-sensitized TiO_2 particles as light harvesters, since reversible binding of an axial pyridine significantly aids catalytic performance.[59,61] CV of **CoP³** on mesoITO electrodes also displayed stable attachment in aqueous solution due to the positioning of the anchoring group in the equatorial ligand backbone.

Despite the stable attachment between **CoP²** and **CoP³** on the ITO surface, prolonged negative polarization of ITO electrodes in aqueous conditions at potentials suitable for H_2 production results in degradation of ITO.[75] Transparent metal oxide semiconductors such as SnO_2 and TiO_2 offer conductivity at potentials more negative than their conduction band (approximately 0.0 V and −0.5 V vs NHE at pH 7,[76] respectively). Moreover, they exhibit improved stability at an applied cathodic potential and can be deposited on fluorine-doped tin oxide (FTO) substrates, which also offer improved stability compared to ITO.[77] Additionally, thin layers of TiO_2[78] and ZrO_2[79] can be deposited on less-stable ITO surfaces to protect them from contact with the electrolyte solution and hence degradation under reducing conditions. The conduction band potentials of these semiconductors are suitable for long-term fuel production by molecular electrocatalysts, since they are less negative than the potentials required for driving reactions such as proton reduction at modest overpotentials. However, electrodes based on semiconducting materials are insulating at potentials within their band gaps, preventing electrochemical characterization of the redox events in this potential region and therefore limiting the mechanistic

DOI: 10.1021/acscatal.7b00326
ACS Catal. 2017, 7, 3131−3141

information available. *In operando* UV/vis spectroelectrochemistry during long-term electrocatalysis can assist in understanding catalytic mechanism on the semiconducting electrodes, for instance by identifying the catalytically active oxidation state.[35]

Ni bis(diphosphine) compounds bearing pendant amine groups have emerged as among the most efficient molecular proton reduction catalysts.[80,81] The pendant amine group in the secondary coordination sphere allows transport of protons to and from the Ni center, as well as stabilizing the nascent H−H bond during hydrogen formation.[13,21] This bioinspired feature is believed to be the key for the observed rates of H_2 production that can match those of hydrogenases under certain conditions.[80]

The nickel bis(diphosphine) catalyst **NiP** (Figure 3) incorporates phosphonic acid groups in the outer coordination sphere, enabling attachment to dye-sensitized metal oxide particles for efficient photocatalytic H_2 production in aqueous suspension.[82] This affinity of **NiP** for TiO_2 has also allowed **NiP** to be implemented in a PEC cell, with mesoporous TiO_2 (mesoTiO_2) being employed instead of ITO as a cathode material coupled to a water-oxidizing iron catalyst-modified WO_3 electrode as the light-harvesting photoanode.[30,83] Mesoporous TiO_2 films were prepared with a thickness of 4 μm and were loaded with **NiP** by immersion in a methanol solution to yield a catalyst coverage of 15 nmol cm^{-2} (geometric area). These catalyst-modified mesoTiO_2|**NiP** electrodes achieved 600 turnovers of Ni-based H_2 production after 8 h at a low overpotential of 250 mV in aqueous electrolyte solution at pH 3.

However, the semiconducting nature of TiO_2 means that the noncatalytic electrochemical properties of the catalyst could not be probed directly. For instance, the CV scans shown in Figure 5A only show charging and, in the absence of **NiP**, discharging of the conduction band (CB). Therefore, electrochemistry and spectroscopy were combined to confirm electron transfer to the **NiP** catalyst via the CB of TiO_2. TiO_2 with a filled CB displays a characteristic blue color with a broad absorbance band in the longer wavelength region of the vis/NIR spectrum.[84] Monitoring the absorbance at λ = 800 nm upon application on −0.43 V vs RHE (Figure 5B) allowed electrons in the CB to be monitored, revealing that the CB was depopulated within seconds of returning to open circuit potential (OCP) in the presence of the catalyst. In the absence of **NiP**, the CB remained populated following electrochemical reduction and return to OCP. It could therefore be concluded that electronic communication between TiO_2 and **NiP** was sufficient to allow rapid electron transfer. The return of the absorbance at 800 nm to its original value suggests that the mononuclear Ni catalyst can depopulate effectively all areas of the mesoporous TiO_2 (average particle size 25 nm), demonstrating the excellent fit and distribution of the small catalyst throughout the porous electrode structure.

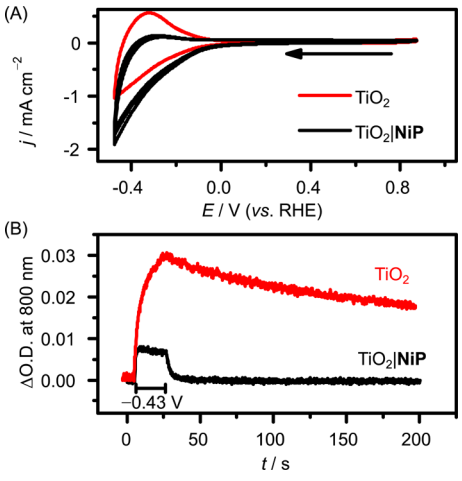

Figure 5. (A) CV scans of TiO_2 modified with **NiP** and (B) spectroelectrochemical study of TiO_2 and TiO_2|**NiP**, monitoring absorbance at 800 nm (CB electrons) before, during, and after application of −0.43 V vs RHE in aqueous electrolyte solution at pH 3. Arrow indicates initial scan direction. Adapted from ref 30.

The integration of phosphonic-acid modified molecular catalysts into metal oxide electrodes has also been used for CO_2 reduction catalysis. A promising class of CO_2 reduction catalysts is that based on the [MnBr(bpy)$(CO)_3$] (bpy = 2,2′-bipyridine) framework.[85] These catalysts are notable for their composition from Earth-abundant elements, as well as low-overpotential and selective CO_2 to CO reduction in the presence of aqueous protons. The good performance is a result of a particular catalytic mechanism, where the initial one electron reduction of two Mn centers is followed by dimerization, and reaction of the Mn^0 dimer with CO_2 to yield two Mn^{II}−CO_2 adducts.[86] Subsequent reduction of Mn^{II} requires a less reducing potential than the first $Mn^I \rightarrow Mn^0$ reduction step, allowing CO production at a low overpotential. Immobilization of a Mn CO_2 reduction catalyst was achieved in a Nafion membrane on a glassy carbon electrode with electrochemical evidence of dimer formation,[41] but since immobilization is often thought to impede dimerization mechanisms,[87] *in operando* spectroelectrochemical studies were required.

The phosphonic acid-bearing Mn catalyst **MnP** (Figure 6A, X = Br) was synthesized for immobilization on metal oxide electrodes.[35] Initially, CV scans with mesoITO electrodes in anhydrous CH_3CN revealed a reversible reduction wave at −1.6 V vs Fc^+/Fc with linear scan rate dependence, demonstrating the presence of immobilized **MnP** with good electronic communication. MesoTiO_2 was used for long-term assessment of CO production activity and selectivity, and CV of these TiO_2|**MnP** electrodes revealed enhanced current at potentials more negative than −1.6 V vs Fc^+/Fc in the presence of CO_2 in CH_3CN/H_2O (19/1). Prolonged CO production by controlled potential electrolysis at −1.7 V vs Fc^+/Fc achieved a TON of 112 per Mn center after 2 h, and this low overpotential is indicative of a one electron reduction followed by dimerization mechanism.[86,88] However, the lack of conductivity within the band gap of TiO_2 prevented characterization of these steps by purely electrochemical techniques, necessitating UV/vis spectroelectrochemistry for further mechanistic insights.

Under catalytic conditions, peaks at 650 and 800 nm were observed (Figure 6B). These bands are characteristic for the formation of a Mn^0−Mn^0 dimer,[85] and it could therefore be inferred that dynamic binding of the phosphonates on TiO_2 was sufficient for a Mn−Mn dimer to form and allow the solution mechanism to be translated to the heterogenized system. These bands disappeared upon return to OCP under CO_2, suggesting that the dimer reacts with CO_2.[85] Therefore, it could be argued that the high local concentration of Mn centers (34 nmol Mn per cm^2 geometric surface area) within the mesoporous TiO_2 promotes catalytically productive dimerization and that future systems can be engineered to promote low-

DOI: 10.1021/acscatal.7b00326
ACS Catal. 2017, 7, 3131−3141

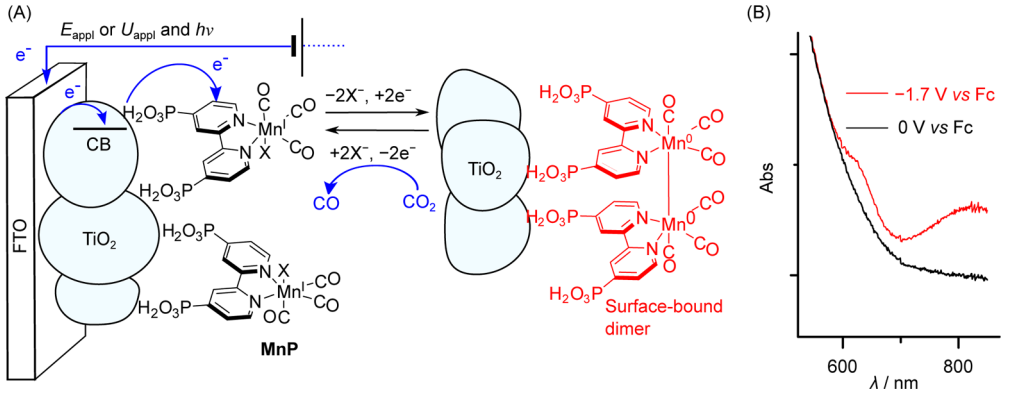

Figure 6. (A) Proposed mechanism for CO_2 reduction by TiO_2|**MnP**. (B) *In operando* UV/vis spectroelectrochemistry of TiO_2|**MnP** in CH_3CN/H_2O (19/1) electrolyte solution under CO_2 revealing dimer formation. Adapted from ref 35.

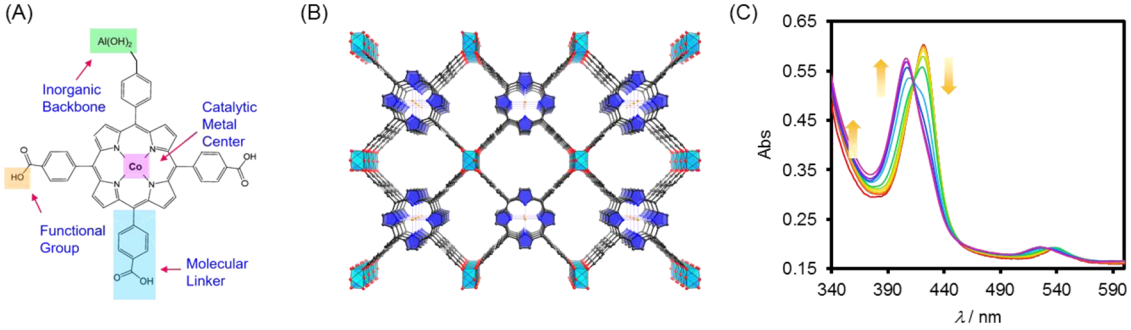

Figure 7. (A) Structure of Co porphyrin catalytic center and (B) overall structure of the Co MOF discussed in section 2.2. (C) Spectroelectrochemistry of the Co porphyrin MOF on FTO scanning from 0.2 V vs RHE (λ_{max} = 422 nm, Co^{II}) to −0.7 V vs RHE (λ_{max} = 408 nm, Co^{I}) in 0.5 M K_2CO_3 electrolyte under CO_2. Adapted with permission from ref 104. Copyright 2015 American Chemical Society.

overpotential bimolecular catalysis through dynamic immobilized molecular catalysts. Having successfully immobilized the Mn catalyst, mesoTiO_2|**MnP** was then combined with a CdS photoanode in a solar-driven CO production PEC cell with an otherwise light-unstable catalyst.

Phosphonic acid-modified analogs of [ReBr(bpy)$(CO)_3$] CO_2 reduction catalysts have been reported,[89−91] including a system comprising an immobilization Re catalyst on TiO_2-protected Cu_2O photocathodes, with the catalytic mechanism studied spectroelectrochemically on bare TiO_2 electrodes.[92] These TiO_2 cathodes modified with the Re catalyst achieved over 70 turnovers for CO production with an applied potential of −2.05 V vs Fc^+/Fc in CH_3CN (overpotential, η = 0.77 V[93,94]) after 1.5 h without irradiation, with a Faradaic efficiency in excess of 80%. Upon application of −1.9 V vs Fc^+/Fc in CH_3CN solution under Ar, peaks at 507 and 578 nm were observed in the UV/vis spectrum and assigned to formation of the doubly reduced Re catalyst. When the measurement was performed under CO_2, the peaks were not observed to the same extent, suggesting that in contrast to the Mn analog, only the doubly reduced species reacts with CO_2, corroborating the observed more negative potential required to drive CO_2 reduction.

2.2. Metal−Organic Framework Materials. Metal−organic frameworks (MOFs) are an effective way of combining molecular components in an extended structure, and they have recently been used to immobilize molecular catalysts on electrode surfaces.[95,96] Also included within this class are one- and two-dimensional polymers comprising dithiolene[97,98] and selenloate[99] ligands coordinated to Co and Ni. These extended polymeric materials have metal centers in well-defined coordination environments and perform electrocatalytic H_2 production under acidic conditions, reaching a current density of 10 mA cm^{-2} at a low overpotential of 343 mV.[99]

Several examples of electrocatalytic fuel formation with MOF-based catalysts involve the reduction of CO_2, since MOFs offer high porosity and accessible sites for chemisorption and as such are often studied for CO_2 uptake and storage.[100−103] The high local CO_2 concentration inside the MOF potentially allows for high activity and selectivity.

A notable example of a MOF for electrocatalytic CO_2 reduction comprised iron tetra-4-carboxyphenyl porphyrin units linked by $Zr_6(\mu_3\text{-}O)_4(\mu_3\text{-}OH)_4$ nodes deposited by electrophoresis on FTO-coated glass electrodes.[87] This system achieved a TON of 272 for electrocatalytic CO production (F.E. = approximately 50%) from CO_2 in acetonitrile electrolyte solution at an applied potential of −1.3 V vs NHE (η = 0.65 V) after 4 h. An important feature of these electrodes was that the Fe centers acted as redox mediators as well as catalytic centers, allowing conductivity of charges across approximately 900 layers and enabling large current densities of up to 5 mA cm^{-2}, which is much higher than would be achievable with a molecular monolayer. Another significant advantage of the use of MOF-based electrocatalytic films, alongside the high local CO_2 concentration, is that they can be grown on transparent conducting substrates and therefore studied by transmission UV/vis spectroelectrochemistry, enabling electrochemical communication across the relatively thick films to be demonstrated. Upon application of a negative electrochemical potential, the Fe^{III} was almost quantitatively

DOI: 10.1021/acscatal.7b00326
ACS Catal. 2017, 7, 3131−3141

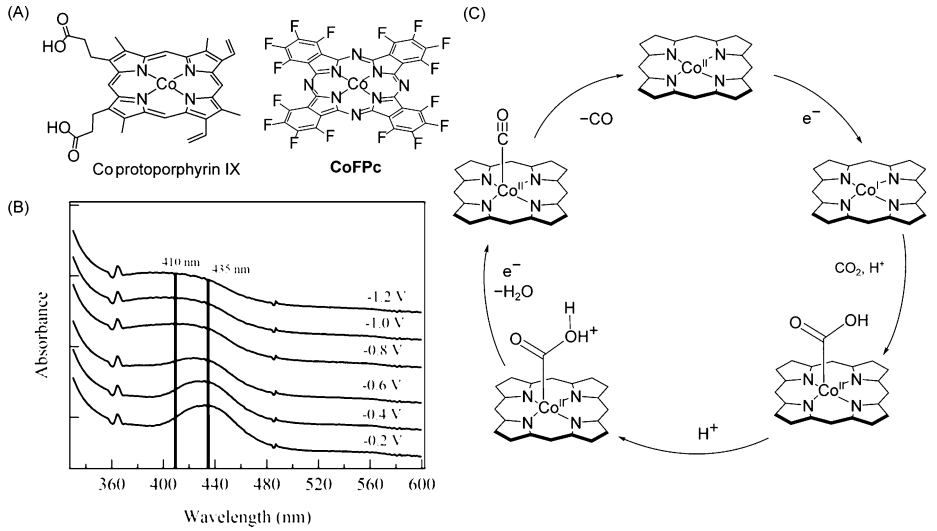

Figure 8. (A) Structures of Co macrocyclic CO_2 reduction catalysts. (B) UV/vis spectroelectrochemistry of electropolymerized Co protoporphyrin IX on FTO under CO_2 (potentials relative to Ag/AgCl reference electrode). Reprinted with permission from ref 58. Copyright 2016 Wiley-VCH Verlag GmbH & Co. KGaA. (C) Proposed scheme for the reduction of CO_2 by Co macrocyclic compounds.[5,58]

reduced to Fe^{II}, and the corresponding reduction in absorbance at 419 nm and increase at 441 nm was observed. Therefore, spectroelectrochemical characterization was able to explain the high current densities. However, the charge transport rate associated with the $Fe^{I/0}$ redox couple was found to be 20 times slower than the $Fe^{III/II}$ couple, highlighting conductivity as a limitation of the use of thick MOF films in catalysis.

Following this report, a number of metal[104]- and covalent-organic frameworks[105] based on cobalt porphyrins have successfully achieved electrocatalytic CO_2 reduction in aqueous conditions. A specific challenge of using electrocatalytic MOF films in aqueous solution is that such materials are sometimes unstable with respect to hydrolysis of metal−ligand coordination bonds, potentially limiting their long-term applicability.[106,107] These challenges were overcome by preparation of a thin-film MOF, synthesized by incorporation of Co porphyrin units into an atomic layer deposition film of alumina (Figure 7A-B).[104] This was found to be active for CO_2 reduction, achieving a turnover number of 1400 per Co center for CO production at a Faradaic efficiency of approximately 50% in aqueous solution (0.5 M K_2CO_3) with an applied potential of −0.7 V vs RHE (η = 0.58 V[105]) after 7 h, with no observed loss of activity during this period. *In situ* spectroelectrochemical studies identified the formation of Co^I under catalytic conditions (Figure 7C), suggesting this to be the active species. Most importantly, complete conversion from Co^{II} to Co^I was observed under reductive conditions, demonstrating that all Co centers were in electronic communication with the surface, improving on the respectable 77% in the Fe porphyrin example,[87] and thus that efficient use was made of the catalyst. However, when thicker films were prepared by performing more ALD cycles, the observed current density was lower, presumably due to poorer charge transport.

2.3. Immobilization by Polymerization. Electropolymerization is a widely used strategy for immobilizing molecular catalysts,[108] utilizing monomers consisting of a catalytic core and a functional group susceptible to polymerization upon application of an electrochemical potential. The resultant films often contain multiple layers of catalysts with limited conductivity, rendering electrochemical studies challenging.[57] However, these films can offer attractive catalytic activity for water oxidation[109] and CO_2 reduction,[110,111] and therefore it is important to gain insights into their mechanism by other complementary techniques. For instance, in the case of a cobalt protoporphyrin IX (Figure 8A), electropolymerization on glassy carbon and FTO electrodes was achieved by oxidation of the vinyl groups.[58] CO_2 reduction with an onset of −1.25 V vs Ag/AgCl was observed in the cyclic voltammogram, but no redox waves assignable to cobalt or ligand-centered reductions were observed at less negative potentials, preventing electrochemical characterization of the catalytically active species. Instead, UV/vis spectroelectrochemistry was used to monitor the oxidation states responsible for CO_2 reduction, and the resultant spectra are shown in Figure 8B. The disappearance of the peak at 435 nm at −0.8 V vs Ag/AgCl indicated reduction of Co^{II}, and the increase in the absorbance at 410 nm was assigned to the formation of Co^I at this potential, which is purported to then react with CO_2. This reaction with CO_2 is believed to be the rate-determining step, due to the accumulation of the peak at 410 nm (Co^I), which is to be expected given the expedited electron transfer with an immobilized species. Therefore, UV/vis spectroelectrochemistry was used to assist the proposal of the mechanism for CO_2 reduction by Co porphyrins and related macrocycles shown in Figure 8C.

2.4. Direct Hydrophobic Immobilization of Unfunctionalized Molecules. A simple and useful route to hybrid electrodes is to use hydrophobic interactions between water-insoluble catalysts and conducting surfaces.[112−115] This strategy does not require synthetic modification of the catalyst core, so it is straightforward to implement as well as avoiding the possible negative effects sometimes observed when installing chemical anchoring groups.[116] Moreover, this offers more freedom for enhancing catalytic activity by synthetic modification of the ligand, as is illustrated below.

Insights gained from *in situ* spectroelectrochemistry have been used to explain improved catalyst design. For cobalt(II) phthalocyanine compound **CoFPc** (Figure 8A) immobilized on carbon cloth electrodes,[5] a discernible reduction wave in the cyclic voltammogram was observed at −0.3 V vs RHE, assigned

DOI: 10.1021/acscatal.7b00326
ACS Catal. 2017, 7, 3131−3141

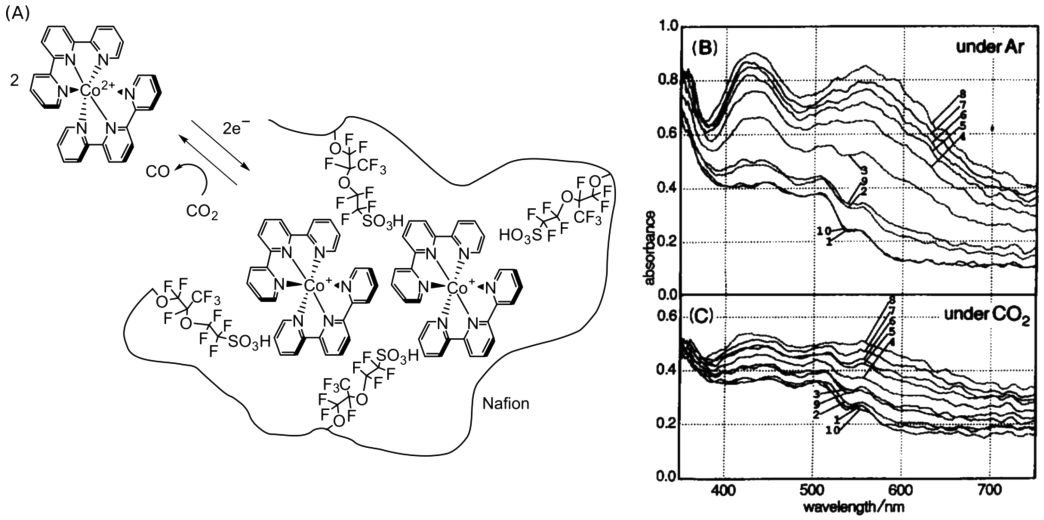

Figure 9. (A) Schematic representation for the electroreduction of CO_2 by $(Co(tpy)_2)^{2+}$. (B) and (C) Reflectance UV/vis spectroelectrochemistry of the $Co(tpy)_2$/Nafion electrode at different points of a CV scan under Ar and CO_2, respectively. Spectra 1−7 denote cathodic scan, 8−10 anodic scan. B and C reprinted with permission from ref 118. Copyright 1993 Elsevier.

to the reduction of Co^{II} to Co^{I}. Under CO_2, this wave was cathodically shifted to −0.5 V vs RHE and was accompanied by electrocatalytic CO production. A spectrum under CO_2 saturated conditions at −0.5 V vs RHE revealed the presence of Co^{I}, establishing the reaction between Co^{I} and CO_2 as the rate-determining step, as with the electropolymerized Co porphyrin. This reduction occurred at a potential approximately 150 mV less negative than for the nonfluorinated analog of **CoFPc** (F atoms replaced with H), and led to significantly improved performance and selectivity for CO over H_2 production compared to the unmodified compound, when compared at the same applied potential. The proposed reason for the improvement was that at low overpotential, a higher proportion of Co centers on a **CoFPc** electrode will be in the reduced state ready to enter the catalytic cycle compared to the less easily reduced unmodified compound, leading to higher current densities.[5,117] This improvement was therefore achieved through identification of the rate-determining step by spectroelectrochemistry and subsequent modification of the molecular catalyst.

The examples described above show largely the same catalytic mechanisms for the immobilized molecular catalyst as in solution, but this should not be automatically assumed as illustrated by the following system. A simple strategy to confine molecules to an electrode surface is to embed them within a membrane that prevents free diffusion of the catalyst but allows the diffusion of catalytic substrates such as protons, H_2O and CO_2, as well as products.[40] The most widely used example is Nafion, which is a fluoropolymer bearing sulfonate groups and therefore allowing cation permeability. In an early example, the CO_2 reduction catalyst $[Co(tpy)_2](PF_6)_2$ (tpy = 2,2′:6′,2″-terpyridine) was incorporated in a 3.6 μm-thick layer of Nafion 117 (Figure 9A).[118] This enabled CO_2 reduction to formate in aqueous phosphate buffer conditions (pH 7), which are not accessible to the molecule in homogeneous solution due to lack of solubility. It was possible to perform *in situ* reflectance spectroelectrochemical characterization of the catalyst, resulting in the spectra shown in Figure 9B−C. At applied potentials more negative than −1.0 V vs SCE, peaks at 430 and 560 nm revealed the formation of $[Co(tpy)_2]^{+}$. When this measurement was performed under CO_2, these peaks did not form to the same extent, indicating that $[Co(tpy)_2]^{+}$ does not accumulate under these conditions and is the species that reacts with CO_2. This stands in contrast to the nonaqueous homogeneous case, where the doubly reduced Co^{0} species reacts with CO_2.[119] It was therefore suggested that the high local concentration of Co^{I} in the membrane under reducing conditions allows a cooperative mechanism where two singly reduced Co^{I} centers combine to react with CO_2. A similar dimerization mechanism with a Mn catalyst embedded in a Nafion membrane has also been suggested,[41] but in neither case was a dimeric species observed directly. Mechanisms such as these and the TiO_2|**MnP** described above (Figure 6),[35] where the reducing equivalents required for catalysis are distributed over multiple centers help to minimize the overpotential requirement, demonstrating the advantages of immobilization of molecular catalysts.

3. MOLECULAR INTEGRITY OF CATALYSTS

A key challenge in molecular electrocatalysis is to demonstrate that the catalytically active species retains its molecular structure.[120,121] Therefore, if the above conclusions are to be drawn and the advantages of molecular structure retained, positive identification of structural integrity is essential.

The *in situ* experiments described above give strong evidence of truly molecular catalysis. In most cases, reduced species with well-defined electronic spectra could be identified under catalytic conditions and assigned by analogy to isolated, solution-based molecular compounds, thus asserting their molecular integrity. Moreover, these reduced species were identified as being catalytically active by either returning to OCP[35] or performing the experiment under CO_2 (Figure 9)[118] and observing the consumption of the reduced species, providing positive evidence that the molecular compound performs catalysis.

Identification of a catalytically active species by UV/vis spectroscopy does not, however, rule out the possibility of an additional decomposed catalyst supplementing the observed activity. High catalytic activity has been observed even with very small amounts of deposited materials,[122] and these are typically not detectable by the techniques used to characterize immobilized molecular compounds such as UV/vis spectroscopy.[123] The techniques used to characterize deposits, typically

DOI: 10.1021/acscatal.7b00326
ACS Catal. 2017, 7, 3131−3141

X-ray photoelectron spectroscopy (XPS) and electron microscopies, must therefore also be employed to check for such materials. The literature regarding decomposition of molecular materials to catalytically active deposits has been well reviewed in terms assessing the stability of molecular catalysts[124] and as a method to producing active materials in its own right.[125] In this case, we shall thus just consider one example where a number of techniques were combined to prove the integrity of the molecular catalyst.

The use of the molecular catalyst **NiP** immobilized on TiO_2 was discussed as an effective H_2-producing cathode above.[30] Since the molecular catalyst itself was not probed directly by *in situ* spectroelectrochemistry, the molecular integrity was instead probed by *ex situ* experiments after H_2 production. First, XPS measurements showed no change in the Ni peak position after electrolysis, with no new signal indicating the presence of reduced Ni^0 nanoparticles. Additionally, the ratios of the elements Ni, P, and N were as expected from the molecular stoichiometry after H_2 production, whereas decomposition to a metallic deposit might be expected to be accompanied by lower amounts of N and P. The molecular structure of the Ni species was qualitatively assessed after catalysis by diffuse reflectance UV/vis and attenuated total reflectance infrared (ATR-IR) spectroscopies. Retention of the Ni d-d electronic transition at 520 nm in the diffuse reflectance UV/vis spectrum indicated the presence of Ni^{II} in the tetraphosphine coordination environment (Figure 3), and signals corresponding to P═O bonds in the ATR-IR spectrum demonstrated the presence of this moiety in the ligand. Therefore, the combined lack of evidence for a decomposed species in the XPS spectra of the hybrid electrode after electrolysis with positive characterization of the molecular catalyst by XPS, UV/vis, and IR spectroscopies provided strong evidence for the molecular integrity of the immobilized catalyst. Similar *ex situ* experiments have also been used to assert the molecular integrity of immobilized CO_2 reduction electrocatalysts.[117]

4. CONCLUSIONS AND OUTLOOK

Immobilization of molecular catalysts on high surface area electrodes has emerged as an attractive strategy for accessing high performance for fuel forming reactions and is also an attractive target for other chemical redox reactions. However, only recently has it become more common place to complement the ubiquitous electrochemical techniques used to study these systems with *in operando* spectroscopic tools. These examples have mainly used UV/vis spectroelectrochemistry, owing to the use of optically transparent electrode materials and transition metal catalysts with distinct spectroscopic handles. The combination of potential-controlled redox chemistry with time-resolved spectroscopy has been powerful and gave valuable insights into catalyst stability and the catalytic process itself, in particular with regard to the mechanism. Study of electron transfer pathways at the electrode/molecule interface has revealed the extent of electronic coupling between the two – particularly highlighting cases where the entire sample of molecular catalyst is electrochemically addressable and therefore catalytically productive. Probing of the catalysts themselves has allowed mechanistic information to be inferred *de novo* under the new chemical environments experienced by the catalysts upon immobilization. Of particular importance has been spectroelectrochemical identification of catalytic "slow steps" – immobilization often expedites electron transfer processes, and therefore diffusion-limited steps such as CO_2 binding and activation become rate-limiting. This insight has enabled ligand modification to improve the catalytic activity, a key advantage of using well-defined molecular components. Finally, these techniques have helped identifying and characterizing examples where, following initial one electron reduction, a dimerization of two catalyst centers has been proposed. This is traditionally thought to be impeded by immobilization but can occur by using more dynamic anchoring strategies such as phosphonic acids and polymer membranes allowing catalytic centers to cooperate. This may open up possibilities for immobilizing other catalysts with bimolecular mechanisms that had previously been thought to be impeded by the lack of translational motion.

We hope that these recent advances in mechanistic understanding of molecular single-site catalysis on electrode surfaces systems will lead to renewed appreciation of molecular systems. They allow the key advantage of using such catalysts – the ability to probe mechanism and alter the molecular structure accordingly – to be retained while implementing catalysts in surface-bound, high turnover conditions that are beginning to match those of solid-state counterparts. It is now envisaged that more sophisticated vibrational spectroscopies will also be applied to such systems, which can lead to further insights and advances toward achieving efficient electrocatalytic fuel production. For example, surface-enhanced resonance Raman spectroscopy has been combined with electrochemistry to study the O_2 and H_2O_2 reduction reactions,[37,38] and this could provide inspiration for the reactions considered in this Perspective.

AUTHOR INFORMATION

Corresponding Author

*E-mail: reisner@ch.cam.ac.uk.

ORCID

Erwin Reisner: 0000-0002-7781-1616

Notes

The authors declare no competing financial interest.

ACKNOWLEDGMENTS

This work was supported by the Christian Doppler Research Association (Austrian Federal Ministry of Science, Research, and Economy and the National Foundation for Research, Technology and Development) the OMV Group, and the EPSRC (DTA studentship to T.E.R.). We thank Dr. Nikolay Kornienko, Dr. Khoa Ly, and Janina Willkomm for helpful discussions.

REFERENCES

(1) Andreiadis, E. S.; Chavarot-Kerlidou, M.; Fontecave, M.; Artero, V. *Photochem. Photobiol.* **2011**, *87*, 946–964.
(2) Lai, Y.-H.; Palm, D. W.; Reisner, E. *Adv. Energy Mater.* **2015**, *5*, 1501668.
(3) Wang, Q.; Hisatomi, T.; Jia, Q.; Tokudome, H.; Zhong, M.; Wang, C.; Pan, Z.; Takata, T.; Nakabayashi, M.; Shibata, N.; Li, Y.; Sharp, I. D.; Kudo, A.; Yamada, T.; Domen, K. *Nat. Mater.* **2016**, *15*, 611–615.
(4) Scholes, G. D.; Fleming, G. R.; Olaya-Castro, A.; van Grondelle, R. *Nat. Chem.* **2011**, *3*, 763–774.
(5) Morlanés, N.; Takanabe, K.; Rodionov, V. *ACS Catal.* **2016**, *6*, 3092–3095.
(6) Willkomm, J.; Muresan, N. M.; Reisner, E. *Chem. Sci.* **2015**, *6*, 2727–2736.

DOI: 10.1021/acscatal.7b00326
ACS Catal. 2017, 7, 3131–3141

(7) Pucino, M.; Mougel, V.; Schowner, R.; Fedorov, A.; Buchmeiser, M. R.; Copéret, C. *Angew. Chem., Int. Ed.* **2016**, *55*, 4300−4302.
(8) Pickett, C. J.; Talarmin, J. *Nature* **1985**, *317*, 652−653.
(9) Yandulov, D. V.; Schrock, R. R. *Science* **2003**, *301*, 76−78.
(10) Zhou, X.; Li, F.; Li, X.; Li, H.; Wang, Y.; Sun, L. *Dalton Trans.* **2015**, *44*, 475−479.
(11) Wombwell, C.; Caputo, C. A.; Reisner, E. *Acc. Chem. Res.* **2015**, *48*, 2858−2865.
(12) Mersch, D.; Lee, C.-Y.; Zhang, J. Z.; Brinkert, K.; Fontecilla-Camps, J. C.; Rutherford, A. W.; Reisner, E. *J. Am. Chem. Soc.* **2015**, *137*, 8541−8549.
(13) Wilson, A. D.; Newell, R. H.; McNevin, M. J.; Muckerman, J. T.; Rakowski DuBois, M.; DuBois, D. L. *J. Am. Chem. Soc.* **2006**, *128*, 358−366.
(14) Cohen, S. M.; Zhang, Z.; Boissonnault, J. A. *Inorg. Chem.* **2016**, *55*, 7281−7290.
(15) Weber, K.; Krämer, T.; Shafaat, H. S.; Weyhermüller, T.; Bill, E.; van Gastel, M.; Neese, F.; Lubitz, W. *J. Am. Chem. Soc.* **2012**, *134*, 20745−20755.
(16) Wombwell, C.; Reisner, E. *Chem. - Eur. J.* **2015**, *21*, 8096−8104.
(17) Healy, A. J.; Ash, P. A.; Lenz, O.; Vincent, K. A. *Phys. Chem. Chem. Phys.* **2013**, *15*, 7055−7059.
(18) Ash, P. A.; Hidalgo, R.; Vincent, K. A. *ACS Catal.* **2017**, *7*, 2471−2485.
(19) Paengnakorn, P.; Ash, P. A.; Shaw, S.; Danyal, K.; Chen, T.; Dean, D. R.; Seefeldt, L. C.; Vincent, K. A. *Chem. Sci.* **2017**, *8*, 1500−1505.
(20) Ash, P. A.; Vincent, K. A. *Chem. Commun.* **2012**, *48*, 1400−1409.
(21) Lubitz, W.; Ogata, H.; Rudiger, O.; Reijerse, E. *Chem. Rev.* **2014**, *114*, 4081−4148.
(22) Spangler, N. J.; Lindahl, P. A.; Bandarian, V.; Ludden, P. W. *J. Biol. Chem.* **1996**, *271*, 7973−7977.
(23) Pinaud, B. A.; Benck, J. D.; Seitz, L. C.; Forman, A. J.; Chen, Z.; Deutsch, T. G.; James, B. D.; Baum, K. N.; Baum, G. N.; Ardo, S.; Wang, H.; Miller, E.; Jaramillo, T. F. *Energy Environ. Sci.* **2013**, *6*, 1983−2002.
(24) McKone, J. R.; Lewis, N. S.; Gray, H. B. *Chem. Mater.* **2014**, *26*, 407−414.
(25) Kasap, H.; Caputo, C. A.; Martindale, B. C. M.; Godin, R.; Lau, V. W.; Lotsch, B. V.; Durrant, J. R.; Reisner, E. *J. Am. Chem. Soc.* **2016**, *138*, 9183−9192.
(26) Martindale, B. C. M.; Joliat, E.; Bachmann, C.; Alberto, R.; Reisner, E. *Angew. Chem., Int. Ed.* **2016**, *55*, 9402−9406.
(27) Lin, C.-Y.; Lai, Y.-H.; Mersch, D.; Reisner, E. *Chem. Sci.* **2012**, *3*, 3482−3487.
(28) Fan, K.; Li, F.; Wang, L.; Daniel, Q.; Gabrielsson, E.; Sun, L. *Phys. Chem. Chem. Phys.* **2014**, *16*, 25234−25240.
(29) Li, F.; Fan, K.; Xu, B.; Gabrielsson, E.; Daniel, Q.; Li, L.; Sun, L. *J. Am. Chem. Soc.* **2015**, *137*, 9153−9159.
(30) Rosser, T. E.; Gross, M. A.; Lai, Y.-H.; Reisner, E. *Chem. Sci.* **2016**, *7*, 4024−4035.
(31) Sherman, B. D.; Sheridan, M. V.; Wee, K.-R.; Marquard, S. L.; Wang, D.; Alibabaei, L.; Ashford, D. L.; Meyer, T. J. *J. Am. Chem. Soc.* **2016**, *138*, 16745−16753.
(32) Kang, P.; Chen, Z.; Nayak, A.; Zhang, S.; Meyer, T. J. *Energy Environ. Sci.* **2014**, *7*, 4007−4012.
(33) Huan, T. N.; Jane, R. T.; Benayad, A.; Guetaz, L.; Tran, P. D.; Artero, V. *Energy Environ. Sci.* **2016**, *9*, 940−947.
(34) Muresan, N. M.; Willkomm, J.; Mersch, D.; Vaynzof, Y.; Reisner, E. *Angew. Chem., Int. Ed.* **2012**, *51*, 12749−12753.
(35) Rosser, T. E.; Windle, C. D.; Reisner, E. *Angew. Chem., Int. Ed.* **2016**, *55*, 7388−7392.
(36) Maurin, A.; Robert, M. *Chem. Commun.* **2016**, *52*, 12084−12087.
(37) Sengupta, K.; Chatterjee, S.; Dey, A. *ACS Catal.* **2016**, *6*, 6838−6852.
(38) Reuillard, B.; Ly, K. H.; Hildebrandt, P.; Jeuken, L. J. C.; Butt, J. N.; Reisner, E. *J. Am. Chem. Soc.* **2017**, *139*, 3324−3327.
(39) Joya, K. S.; Sala, X. *Phys. Chem. Chem. Phys.* **2015**, *17*, 21094−21103.
(40) Yoshida, T.; Tsutsumida, K.; Teratani, S.; Yasufuku, K.; Kaneko, M. *J. Chem. Soc., Chem. Commun.* **1993**, 631−633.
(41) Walsh, J. J.; Neri, G.; Smith, C. L.; Cowan, A. J. *Chem. Commun.* **2014**, *50*, 12698−12701.
(42) Reuillard, B.; Warnan, J.; Leung, J. J.; Wakerley, D. W.; Reisner, E. *Angew. Chem., Int. Ed.* **2016**, *55*, 3952−3957.
(43) Delamar, M.; Hitmi, R.; Pinson, J.; Savéant, J. M. *J. Am. Chem. Soc.* **1992**, *114*, 5883−5884.
(44) Allongue, P.; Delamar, M.; Desbat, B.; Fagebaume, O.; Hitmi, R.; Pinson, J.; Savéant, J.-M. *J. Am. Chem. Soc.* **1997**, *119*, 201−207.
(45) Tran, P. D.; Le Goff, A.; Heidkamp, J.; Jousselme, B.; Guillet, N.; Palacin, S.; Dau, H.; Fontecave, M.; Artero, V. *Angew. Chem., Int. Ed.* **2011**, *50*, 1371−1374.
(46) Maurin, A.; Robert, M. *J. Am. Chem. Soc.* **2016**, *138*, 2492−2495.
(47) Queffélec, C.; Petit, M.; Janvier, P.; Knight, D. A.; Bujoli, B. *Chem. Rev.* **2012**, *112*, 3777−3807.
(48) Brennan, B. J.; Llansola Portolés, M. J.; Liddell, P. A.; Moore, T. A.; Moore, A. L.; Gust, D. *Phys. Chem. Chem. Phys.* **2013**, *15*, 16605−16614.
(49) Willkomm, J.; Orchard, K. L.; Reynal, A.; Pastor, E.; Durrant, J. R.; Reisner, E. *Chem. Soc. Rev.* **2016**, *45*, 9−23.
(50) Queyriaux, N.; Kaeffer, N.; Morozan, A.; Chavarot-Kerlidou, M.; Artero, V. *J. Photochem. Photobiol., C* **2015**, *25*, 90−105.
(51) Sun, C.; Gobetto, R.; Nervi, C. *New J. Chem.* **2016**, *40*, 5656−5661.
(52) Le Goff, A.; Artero, V.; Jousselme, B.; Tran, P. D.; Guillet, N.; Métayé, R.; Fihri, A.; Palacin, S.; Fontecave, M. *Science* **2009**, *326*, 1384−1387.
(53) Hoertz, P. G.; Chen, Z.; Kent, C. A.; Meyer, T. J. *Inorg. Chem.* **2010**, *49*, 8179−8181.
(54) Hanson, K.; Torelli, D. A.; Vannucci, A. K.; Brennaman, M. K.; Luo, H.; Alibabaei, L.; Song, W.; Ashford, D. L.; Norris, M. R.; Glasson, C. R. K.; Concepcion, J. J.; Meyer, T. J. *Angew. Chem., Int. Ed.* **2012**, *51*, 12782−12785.
(55) Gross, M. A.; Creissen, C. E.; Orchard, K. L.; Reisner, E. *Chem. Sci.* **2016**, *7*, 5537−5546.
(56) Li, H.; Li, F.; Wang, Y.; Bai, L.; Yu, F.; Sun, L. *ChemPlusChem* **2016**, *81*, 1056−1059.
(57) Abruña, H. D. *Coord. Chem. Rev.* **1988**, *86*, 135−189.
(58) Pander, J. E., III; Fogg, A.; Bocarsly, A. B. *ChemCatChem* **2016**, *8*, 3536−3545.
(59) Razavet, M.; Artero, V.; Fontecave, M. *Inorg. Chem.* **2005**, *44*, 4786−4795.
(60) Hu, X.; Brunschwig, B. S.; Peters, J. C. *J. Am. Chem. Soc.* **2007**, *129*, 8988−8998.
(61) Wakerley, D. W.; Reisner, E. *Phys. Chem. Chem. Phys.* **2014**, *16*, 5739−5746.
(62) Lakadamyali, F.; Kato, M.; Reisner, E. *Faraday Discuss.* **2012**, *155*, 191−205.
(63) Andreiadis, E. S.; Jacques, P.-A.; Tran, P. D.; Leyris, A.; Chavarot-Kerlidou, M.; Jousselme, B.; Matheron, M.; Pécaut, J.; Palacin, S.; Fontecave, M.; Artero, V. *Nat. Chem.* **2013**, *5*, 48−53.
(64) Lacy, D. C.; Roberts, G. M.; Peters, J. C. *J. Am. Chem. Soc.* **2015**, *137*, 4860−4864.
(65) Anxolabéhère-Mallart, E.; Costentin, C.; Fournier, M.; Nowak, S.; Robert, M.; Savéant, J.-M. *J. Am. Chem. Soc.* **2012**, *134*, 6104−6107.
(66) Anxolabéhère-Mallart, E.; Costentin, C.; Fournier, M.; Robert, M. *J. Phys. Chem. C* **2014**, *118*, 13377−13381.
(67) Donck, S.; Fize, J.; Gravel, E.; Doris, E.; Artero, V. *Chem. Commun.* **2016**, *52*, 11783−11786.
(68) Bae, E.; Choi, W. *J. Phys. Chem. B* **2006**, *110*, 14792−14799.
(69) Lakadamyali, F.; Reisner, E. *Chem. Commun.* **2011**, *47*, 1695−1697.
(70) Lakadamyali, F.; Kato, M.; Muresan, N. M.; Reisner, E. *Angew. Chem., Int. Ed.* **2012**, *51*, 9381−9384.
(71) Lakadamyali, F.; Reynal, A.; Kato, M.; Durrant, J. R.; Reisner, E. *Chem. - Eur. J.* **2012**, *18*, 15464−15475.

DOI: 10.1021/acscatal.7b00326
ACS Catal. 2017, 7, 3131−3141

(72) Wakerley, D. W.; Gross, M. A.; Reisner, E. *Chem. Commun.* **2014**, *50*, 15995−15998.
(73) Scherer, M. R. J.; Muresan, N. M.; Steiner, U.; Reisner, E. *Chem. Commun.* **2013**, *49*, 10453−10455.
(74) Wadsworth, B. L.; Beiler, A. M.; Khusnutdinova, D.; Jacob, S. I.; Moore, G. F. *ACS Catal.* **2016**, *6*, 8048−8057.
(75) Senthilkumar, M.; Mathiyarasu, J.; Joseph, J.; Phani, K. L. N.; Yegnaraman, V. *Mater. Chem. Phys.* **2008**, *108*, 403−407.
(76) Vinodgopal, K.; Bedja, I.; Kamat, P. V. *Chem. Mater.* **1996**, *8*, 2180−2187.
(77) Plá Cid, C. C.; Spada, E. R.; Sartorelli, M. L. *Appl. Surf. Sci.* **2013**, *273*, 603−606.
(78) Alibabaei, L.; Farnum, B. H.; Kalanyan, B.; Brennaman, M. K.; Losego, M. D.; Parsons, G. N.; Meyer, T. J. *Nano Lett.* **2014**, *14*, 3255−3261.
(79) Norris, M. R.; Cossairt, B. M. *J. Mater. Chem. A* **2015**, *3*, 14585−14591.
(80) Helm, M. L.; Stewart, M. P.; Bullock, R. M.; Rakowski Dubois, M.; DuBois, D. L. *Science* **2011**, *333*, 863−866.
(81) Wiese, S.; Kilgore, U. J.; DuBois, D. L.; Bullock, R. M. *ACS Catal.* **2012**, *2*, 720−727.
(82) Gross, M. A.; Reynal, A.; Durrant, J. R.; Reisner, E. *J. Am. Chem. Soc.* **2014**, *136*, 356−366.
(83) Klepser, B. M.; Bartlett, B. M. *J. Am. Chem. Soc.* **2014**, *136*, 1694−1697.
(84) Mohamed, H. H.; Mendive, C. B.; Dillert, R.; Bahnemann, D. W. *J. Phys. Chem. A* **2011**, *115*, 2139−2147.
(85) Bourrez, M.; Molton, F.; Chardon-Noblat, S.; Deronzier, A. *Angew. Chem., Int. Ed.* **2011**, *50*, 9903−9906.
(86) Bourrez, M.; Orio, M.; Molton, F.; Vezin, H.; Duboc, C.; Deronzier, A.; Chardon-Noblat, S. *Angew. Chem., Int. Ed.* **2014**, *53*, 240−243.
(87) Hod, I.; Sampson, M. D.; Deria, P.; Kubiak, C. P.; Farha, O. K.; Hupp, J. T. *ACS Catal.* **2015**, *5*, 6302−6309.
(88) Sampson, M. D.; Nguyen, A. D.; Grice, K. A.; Moore, C. E.; Rheingold, A. L.; Kubiak, C. P. *J. Am. Chem. Soc.* **2014**, *136*, 5460−5471.
(89) Hawecker, J.; Lehn, J.-M.; Ziessel, R. *J. Chem. Soc., Chem. Commun.* **1984**, 328−330.
(90) Windle, C. D.; Pastor, E.; Reynal, A.; Whitwood, A. C.; Vaynzof, Y.; Durrant, J. R.; Perutz, R. N.; Reisner, E. *Chem. - Eur. J.* **2015**, *21*, 3746−3754.
(91) Won, D.-I.; Lee, J.-S.; Ji, J.-M.; Jung, W.-J.; Son, H.-J.; Pac, C.; Kang, S. O. *J. Am. Chem. Soc.* **2015**, *137*, 13679−13690.
(92) Schreier, M.; Luo, J.; Gao, P.; Moehl, T.; Mayer, M. T.; Grätzel, M. *J. Am. Chem. Soc.* **2016**, *138*, 1938−1946.
(93) Costentin, C.; Drouet, S.; Robert, M.; Savéant, J.-M. *Science* **2012**, *338*, 90−94.
(94) Pavlishchuk, V. V.; Addison, A. W. *Inorg. Chim. Acta* **2000**, *298*, 97−102.
(95) Hod, I.; Deria, P.; Bury, W.; Mondloch, J. E.; Kung, C.-W.; So, M.; Sampson, M. D.; Peters, A. W.; Kubiak, C. P.; Farha, O. K.; Hupp, J. T. *Nat. Commun.* **2015**, *6*, 8304.
(96) Ahrenholtz, S. R.; Epley, C. C.; Morris, A. J. *J. Am. Chem. Soc.* **2014**, *136*, 2464−2472.
(97) Downes, C. A.; Marinescu, S. C. *J. Am. Chem. Soc.* **2015**, *137*, 13740−13743.
(98) Downes, C. A.; Marinescu, S. C. *Dalton Trans.* **2016**, *45*, 19311−19321.
(99) Downes, C. A.; Marinescu, S. C. *ACS Catal.* **2017**, *7*, 848−854.
(100) Phan, A.; Doonan, C. J.; Uribe-Romo, F. J.; Knobler, C. B.; O'Keeffe, M.; Yaghi, O. M. *Acc. Chem. Res.* **2010**, *43*, 58−67.
(101) Millward, A. R.; Yaghi, O. M. *J. Am. Chem. Soc.* **2005**, *127*, 17998−17999.
(102) Hinogami, R.; Yotsuhashi, S.; Deguchi, M.; Zenitani, Y.; Hashiba, H.; Yamada, Y. *ECS Electrochem. Lett.* **2012**, *1*, H17−H19.
(103) Senthil Kumar, R.; Senthil Kumar, S.; Anbu Kulandainathan, M. *Electrochem. Commun.* **2012**, *25*, 70−73.
(104) Kornienko, N.; Zhao, Y.; Kley, C. S.; Zhu, C.; Kim, D.; Lin, S.; Chang, C. J.; Yaghi, O. M.; Yang, P. *J. Am. Chem. Soc.* **2015**, *137*, 14129−14135.
(105) Lin, S.; Diercks, C. S.; Zhang, Y.-B.; Kornienko, N.; Nichols, E. M.; Zhao, Y.; Paris, A. R.; Kim, D.; Yang, P.; Yaghi, O. M.; Chang, C. J. *Science* **2015**, *349*, 1208−1213.
(106) Leus, K.; Bogaerts, T.; De Decker, J.; Depauw, H.; Hendrickx, K.; Vrielinck, H.; Van Speybroeck, V.; Van Der Voort, P. *Microporous Mesoporous Mater.* **2016**, *226*, 110−116.
(107) Tan, K.; Nijem, N.; Canepa, P.; Gong, Q.; Li, J.; Thonhauser, T.; Chabal, Y. J. *Chem. Mater.* **2012**, *24*, 3153−3167.
(108) Denisevich, P.; Abruña, H. D.; Leidner, C. R.; Meyer, T. J.; Murray, R. W. *Inorg. Chem.* **1982**, *21*, 2153−2161.
(109) Wang, L.; Fan, K.; Daniel, Q.; Duan, L.; Li, F.; Philippe, B.; Rensmo, H.; Chen, H.; Sun, J.; Sun, L. *Chem. Commun.* **2015**, *51*, 7883−7886.
(110) Hu, X.-M.; Salmi, Z.; Lillethorup, M.; Pedersen, E. B.; Robert, M.; Pedersen, S. U.; Skrydstrup, T.; Daasbjerg, K. *Chem. Commun.* **2016**, *52*, 5864−5867.
(111) Ashford, D. L.; Lapides, A. M.; Vannucci, A. K.; Hanson, K.; Torelli, D. A.; Harrison, D. P.; Templeton, J. L.; Meyer, T. J. *J. Am. Chem. Soc.* **2014**, *136*, 6578−6581.
(112) Brimblecombe, R.; Bond, A. M.; Dismukes, G. C.; Swiegers, G. F.; Spiccia, L. *Phys. Chem. Chem. Phys.* **2009**, *11*, 6441−6449.
(113) Morlanés, N.; Joya, K. S.; Takanabe, K.; Rodionov, V. *Eur. J. Inorg. Chem.* **2015**, *2015*, 49−52.
(114) Chen, B.-T.; Morlanés, N.; Adogla, E.; Takanabe, K.; Rodionov, V. O. *ACS Catal.* **2016**, *6*, 4647−4652.
(115) Li, F.; Li, L.; Tong, L.; Daniel, Q.; Göthelid, M.; Sun, L. *Chem. Commun.* **2014**, *50*, 13948−13951.
(116) Walsh, J. J.; Smith, C. L.; Neri, G.; Whitehead, G. F. S.; Robertson, C. M.; Cowan, A. J. *Faraday Discuss.* **2015**, *183*, 147−160.
(117) Zhang, X.; Wu, Z.; Zhang, X.; Li, L.; Li, Y.; Xu, H.; Li, X.; Yu, X.; Zhang, Z.; Liang, Y.; Wang, H. *Nat. Commun.* **2017**, *8*, 14675.
(118) Yoshida, T.; Iida, T.; Shirasagi, T.; Lin, R.-J.; Kaneko, M. *J. Electroanal. Chem.* **1993**, *344*, 355−362.
(119) Guadalupe, A. R.; Usifer, D. A.; Potts, K. T.; Hurrell, H. C.; Mogstad, A.-E.; Abruña, H. D. *J. Am. Chem. Soc.* **1988**, *110*, 3462−3466.
(120) Wombwell, C.; Reisner, E. *Dalton Trans.* **2014**, *43*, 4483−4493.
(121) Martin, D. J.; McCarthy, B. D.; Donley, C. L.; Dempsey, J. L. *Chem. Commun.* **2015**, *51*, 5290−5293.
(122) Roger, I.; Symes, M. D. *J. Am. Chem. Soc.* **2015**, *137*, 13980−13988.
(123) Daniel, Q.; Ambre, R. B.; Zhang, B.; Philippe, B.; Chen, H.; Li, F.; Fan, K.; Ahmadi, S.; Rensmo, H.; Sun, L. *ACS Catal.* **2017**, *7*, 1143−1149.
(124) Artero, V.; Fontecave, M. *Chem. Soc. Rev.* **2013**, *42*, 2338−2356.
(125) Roger, I.; Symes, M. D. *J. Mater. Chem. A* **2016**, *4*, 6724−6741.

DOI: 10.1021/acscatal.7b00326
ACS Catal. 2017, 7, 3131−3141